Article

Development of Perfluoro Decalin/Fluorinated Polyimide Core−Shell Microparticles via SPG Membrane Emulsification Using Methyl Perfluoropropyl Ether Cosolvent

Qiming Zhang, Natsuko F. Inagaki, Arvind K. Singh Chandel, Hiromi Yoshida, Da Xiao, Masamichi Kamihira, Tomohito Hamada, Shigehito Sagisaka, Yosuke Kishikawa, and Taichi Ito*

Cite This: *ACS Omega* 2024, 9, 21127−21135

Read Online

ACCESS | Metrics & More | Article Recommendations | SI Supporting Information

ABSTRACT: Red blood cell-inspired perfluorocarbon-encapsulated core−shell particles have been developed for biomedical applications. Although the use of perfluorodecalin (FDC) is expected for core−shell particles owing to its high oxygen solubility, the low solubility of FDC in any organic solvent, owing to its fluorous properties, prevents its use in core−shell particles. In this study, a new cosolvent system composed of dichloromethane (DCM) and heptafluoropropyl methyl ether (HFPME) was found to dissolve both FDC and fluorinated polyimide (FPI) based on a systematic study using a phase diagram, achieving a homogeneous disperse phase for emulsification composed of oxygen-permeable FPI and oxygen-soluble FDC. Using this novel cosolvent system and Shirasu porous glass (SPG) membrane emulsification, FDC-encapsulated FPI shell microparticles were successfully prepared for the first time. In addition to oxygenation, demonstrated using hypoxia-responsive HeLa cells, the fabricated core−shell microparticles exhibited monodispersity, excellent stability, biocompatibility, and oxygen capacity.
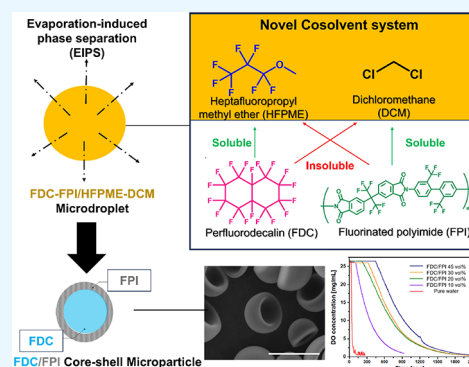
1. INTRODUCTION

Artificial oxygen carriers (AOCs) have been extensively studied as blood substitutes.[1] Recently, AOCs have also been employed in regenerative medicine and tissue engineering.[2] Hemoglobin-based oxygen carriers, such as cross-linked hemoglobin or hemoglobin encapsulated in liposomes and nanodroplets composed of perfluorocarbons (PFCs), have been widely investigated, including in clinical research, owing to their high oxygen solubility.[3−5] Additionally, micrometer-sized oxygen carriers that mimic the shape and function of red blood cells (RBCs) have also been recently studied.[6,7]

RBCs have a core−shell structure in which a highly concentrated aqueous hemoglobin solution is enclosed in a flexible cell membrane.[8] Very recently, we have reported core−shell artificial oxygen carriers with a narrow particle size distribution and a size similar to human RBCs using the Shirasu porous glass (SPG) membrane emulsification technique.[9,10] In particular, we obtained core−shell particles by emulsification of the dispersed phase containing perfluorooctyl bromide (PFOB), a type of PFCs, and poly(lactic acid)/epsilon caprolactam copolymer (PLC) in dichloromethane (DCM), followed by evaporation-induced phase separation (EIPS) and a solidification method.[9] In a similar process, a polydimethylsiloxane thermoplastic elastomer (PDMS-TPE) was used instead of PLC to obtain PFOB/PDMS-TPE core−shell particles as a novel oxygen carrier.[10]

To serve as a shell material for core−shell oxygen carriers, a polymer with excellent oxygen permeability, durability, and biocompatibility is desirable to enable the fast absorption and dissipation of oxygen.[6] Polyimides exhibit excellent gas permeability, and their application in various gas-separation membranes has been extensively investigated.[11] Among them, fluorinated polyimide (FPI) is expected to be applied to artificial lungs due to its high gas permeability, durability, and biocompatibility. Additionally, FPI is soluble in solvents such as chloroform, DCM, and 1,1,2-trichloroethane (TCE), making them excellent for processing applications, such as hollow fiber membrane spinning. The good solubility of FPI in DCM is a major advantage, along with its high acid/alkali durability and oxygen permeability.[12,13]

Several PFCs are envisioned as core materials for core−shell oxygen carriers. In addition to PFOB, perfluorodecalin (FDC), perfluorotripropylamine (FTPA), perfluoro-*N*-methyldecahydroisoquinoline (FMIQ), and bis(perfluorobutyl)ethylene have been considered as candidates for core materials.[14]
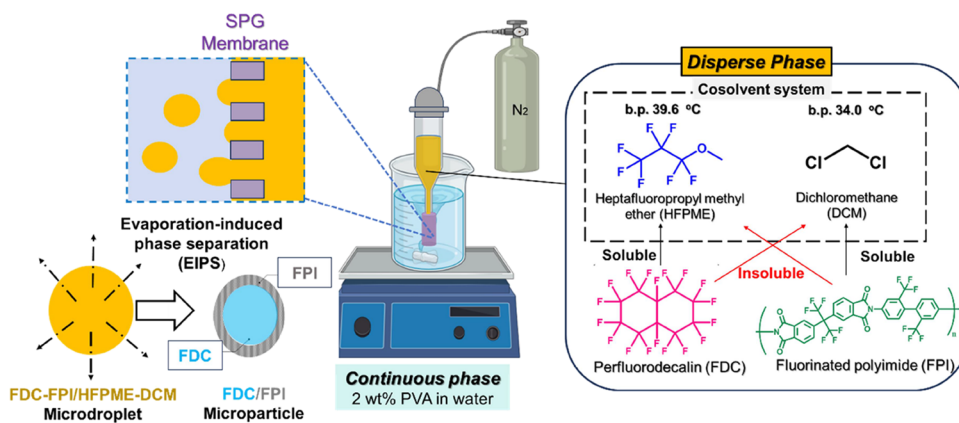
Figure 1. Schematic representation of the FDC/FPI core−shell microparticle preparation through SPG membrane emulsification and EIPS. Both FDC and FPI readily dissolved in the cosolvent system of HFPME (Novec 7000) and DCM, forming a single-phase dispersed phase. This phase was subsequently emulsified by the SPG membrane. The resulting emulsions spontaneously generated FDC/FPI core−shell microparticles through the evaporation of both HFPME (boiling point 34 °C) and DCM (boiling point 40 °C).

PFOB has been utilized in second-generation artificial oxygen carriers, such as Oxygent, and has also been clinically used in vivo as an artificial lung surfactant.[15] FDC, a cyclic PFC used in first-generation artificial oxygen carriers such as Fluosol-DA, is anticipated to become more important in the future due to its environmentally friendly nature. In our previous study, we fabricated FDC microdroplets via SPG membrane emulsification, suggesting their usefulness as microsized oxygen carriers.[16] Unlike PFOB which is soluble in some organic solvents, such as DCM, at low concentrations, FDC is insoluble in common organic solvents. Therefore, developing core−shell oxygen carriers with FDCs through continuous processes involving emulsification, EIPS, and solidification methods is impossible.

In this study, we discovered that heptafluoropropyl methyl ether (HFPME), a type of hydrofluoroether (marketed under the trade name Novec 7000 Engineered Fluid), and DCM were mutually compatible in any ratio. Building upon the observation that this innovative cosolvent effectively dissolved both FDC and FPI, we endeavored to fabricate core−shell microparticles of FDC/FPI, with FPI forming the shell and FDC constituting the core. This was achieved through continuous processes involving SPG membrane emulsification, EIPS, and subsequent solidification. The thickness of the particles, their size, and compression resistance were characterized, and their performance as oxygen carriers was investigated.

2. METHODS

2.1. Materials. FPI, whose chemical structure is shown in Figure 1, was provided by Daikin Industry Co., Ltd. (Osaka, Japan). Poly(vinyl alcohol) (PVA) with a molecular weight (M_w) of 13,000−23,000 kDa and a degree of saponification of 87−89 mol % was purchased from Sigma-Aldrich (St. Louis, MO, USA). HFPME (Novec 7000) was acquired from 3 M (Saint Paul, USA). FDC, hexafluorobenzene, Nile Red, potassium bromide (KBr), DCM, Dulbecco's modified Eagle's medium (DMEM), fetal bovine serum (FBS), penicillin-streptomycin-amphotericin B suspension (PSA), chloroform-d_6, and phosphate-buffered saline (PBS) were obtained from Wako Pure Chemical Industries, Ltd. (Osaka, Japan). Saline was purchased from Otsuka Pharmaceutical Co. Ltd. (Tokyo, Japan). Packed human red blood cells (Ir-RBC-LR-2) were

acquired from the Japanese Red Cross Society with the approval of the Ethics Committee of the Faculty of Medicine, University of Tokyo (10412) and Ministry of Health, Labour, and Welfare, Japan (27J0029).

2.2. Determination of the Ternary Phase Diagrams. The ternary phase diagram of DCM-FDC-HFPME was determined through titration. Various ratios of DCM and the FDC were mixed in vials, and phase separation occurred after the vials were shaken. HFPME was then gradually added using a glass pipet and a pipet gun until the mixture became cloudy and a single phase after shaking.

The cloud-point titration method was applied to the ternary phase system of FPI-DCM-HEPME. Initially, FPI was fully dissolved in DCM, and HEPME was gradually added to the solution, followed by gentle shaking until the solution became cloudy. Ternary phase diagrams were constructed using MATLAB 2021a, based on the experimental miscibility data of the mass fraction at each critical cloud point.

2.3. Preparation of FDC/FPI Core−Shell Microparticles. To prepare core−shell particles, SPG membrane emulsification was conducted using an internal pressure-type module (SPG Technology, Miyazaki, Japan). In this process, 61 μL of FDC, 600 μL of HFPME, and 50 mg of FPI were dissolved in 2 mL of DCM, forming a homogeneous dispersed phase. The phases of the cosolvents of PFCs (e.g., FDC and HFPME), and organic solvents (e.g., DCM), are expressed as O−F. To enable fluorescent observations, 0.1 mg mL^{-1} of Nile red was also incorporated into the disperse phase.

Before commencing emulsification, a hydrophilic SPG membrane (SPG Technology, Miyazaki, Japan) with pore sizes of 4 μm was immersed in a continuous phase consisting of an aqueous 2 wt % PVA solution. This was followed by sonication at room temperature for 1 h. The disperse phase was then emulsified within 20 mL of the continuous phase at 4 °C, employing a stirring speed of 150 rpm. At a critical transmembrane pressure (7.5 kPa), emulsification started at a steady dispersed phase flux of 2 mL h^{-1} without fouling.

The resulting (O−F)/W (W stands for water phase) emulsions were stirred at 300 rpm at room temperature for 4 h to allow complete removal of DCM and HFPME. This led to the formation of core−shell particles through evaporation-induced phase separation. The resulting core−shell particle

suspension was washed three times with pure water and stored at room temperature.

2.4. Characterization of Core−Shell Particles. The morphological characteristics of the core−shell particles obtained were examined using scanning electron microscopy (SEM) (S4700, Hitachi, Tokyo, Japan) and confocal laser scanning microscopy (CLSM) (FV3000; Olympus, Tokyo, Japan). To prepare the washed particles for SEM imaging, they were lyophilized and subsequently affixed to a carbon tape. A thin layer of gold was sputtered onto the samples to ensure proper SEM visualization. Likewise, lyophilized particles were embedded in OCT resin, and cryo-microtomy was performed to obtain 10 μm-thick sections. These sections were sputtered with gold before being utilized for SEM imaging.

An argon laser (514 nm) was used for the excitation. The thickness of the particles' shells was determined from the CLSM images using ImageJ 1.51k software (Wayne Rasband, USA). Fourier-transform infrared (FT-IR) spectra were recorded using an FT-IR spectrometer (FT/IR-4200ST, JASCO). Polymer samples were examined using KBr tablets, whereas liquid PFOB samples were analyzed using NaCl cells. The particle size distribution was assessed using a laser diffraction particle size distribution analyzer (LA-950 V2, Horiba, Kyoto, Japan) by analyzing the diffraction pattern of the irradiated light. To confirm FDC encapsulation inside the FDC/FPI core−shell particles, the particles were freeze-dried and dissolved in chloroform-d_6, and the ^{19}F NMR spectra of the prepared solutions were measured with 32 scans at a relaxation time of 8 s (JEOL JNM-A500, JEOL, Tokyo, Japan).

2.5. Stability of Particles to Acidic and Basic Environments, Autoclave, and Ethanol Sterilization. To assess the pH resistance of the FDC/FPI core−shell particles, a 10 vol % particle suspension was incubated overnight in various aqueous media with the pH adjusted by NaOH or HCl to 3, 4, 5, 6, 7, 8, or 10. To confirm the sterilization ability of the FDC/FPI core−shell particles, the particle suspension was subjected to autoclaving, ethanol immersion, and ethylene oxide (EO) gas sterilization in separate groups. For autoclaving, a 10 vol % FDC/FPI core−shell particle suspension was autoclaved at 121 °C and 2 atm for 20 min (equipment information). For ethanol immersion, a 10 vol % particle suspension in 70% ethanol was incubated overnight at 37 °C. For EO sterilization, a 10 vol % particle suspension in pure water was processed by a standard EO sterilizer (equipment information) for 3 h at 45 °C. Subsequently, the morphology of all the treated groups was examined using SEM, and the encapsulated FDC was confirmed using ^{19}F NMR and FT-IR spectroscopy.

2.6. Oxygenation and Deoxygenation. The deoxygenation and oxygenation processes of the FDC/FPI core−shell particles were assessed by tracking the changes in the dissolved oxygen (DO) concentration over time. To initiate deoxygenation, 20 mL of a suspension of FDC/FPI core−shell particles in pure water (45, 30, 20, and 10%) were initially oxygenated with a 100 mL min^{-1} oxygen feed. Subsequently, the samples were deoxygenated by perfusing nitrogen gas into the suspension at a flow of 100 mL min^{-1}. In the case of oxygenation, an equivalent volume of the sample was first deoxygenated by bubbling it with nitrogen, and then oxygenation was achieved by introducing air at 100 mL min^{-1}. The DO concentration during both the deoxygenation and oxygenation processes was continuously monitored using a DO meter (Visiferm DO ARC 120, Hamilton, Reno, USA)

immersed in the samples. As a control, the DO concentrations of pure water and 10% FDC emulsified with Pluronic F127 were measured throughout the deoxygenation and oxygenation procedures. Three independent experiments were conducted for each condition.

2.7. Assessment of Oxygenation to Hypoxia-Responsive (hr-HeLa) Cells. Hypoxia-responsive hr-HeLa cells are HeLa cells genetically modified to express the EGFP gene in response to hypoxia and were used to evaluate oxygen supply performance.[17] For 2D cell cultures, cells were seeded onto a 24-well glass-bottom plate at a density of 2×10^4 cells per well with 750 μL of culture medium (DMEM, 10% FBS, 1% PSA) and incubated overnight at 37 °C under 20% O$_2$ and 5% CO$_2$ conditions. Following our previously reported procedure,[9,16] cells were seeded on the same plate at a density of 2×10^5 cells per well and maintained at 37 °C under 20% O$_2$ and 5% CO$_2$ conditions for 48 h, growing into a multilayered culture, commonly referred to as 3D cell culture. Subsequently, 500 μL of samples containing cells-to-FDC/FPI core−shell particle ratios of 1:1, 1:2, 1:5, and 1:10 were added to the cells, which were then exposed to 2% O$_2$ and 5% CO$_2$ conditions for an additional 48 h. A CLSM employing red (E$_x$/FL= 560 nm/650 nm) and green emission filters (E$_x$/FL= 488 nm/530 nm) was used to capture CLSM microscopic images of FDC/FPI core−shell particles and hr-HeLa cells respectively in the culture.

3. RESULTS AND DISCUSSION

3.1. Novel Cosolvent System of FDC, DCM, and HFPME. FDC is a perfluorinated decane immiscible in inorganic solvents. We intended to dissolve the FDC in the organic phase, composed of low-boiling-point solvents including DCM that can be easily evaporated. HFPME is frequently used in the semiconductor industry as an organic solvent and has a boiling point of 34 °C. In this study, we focused on the ternary cosolvent systems DCM, FDC, and HFPME, the phase diagrams of which are shown in Figure 2a. We discovered that FDC was miscible with a mixture of DCM and HFPME systems at a certain ratio at room temperature. Since FDC was insoluble in DCM at room temperature before adding HFPME, the mixture was initially separated into two phases. As HFPME was gradually added to the mixture until the cloud point was reached, the two-phase system suddenly coalesced into a single phase at a certain composition. Thus, the binodal line in the ternary phase diagram reveals a critical relationship within the mixture of DCM, FDC, and HFPME (Figure 2a). To the best of our knowledge, this is the first report on this cosolvent system.

3.2. Fabrication of FDC/FPI Core−Shell Particles Using the New Cosolvent System. Based on the new design of FDC/FPI artificial oxygen carriers in this study, both FDC and FPI were solutes in the dispersed phase of SPG membrane emulsification. Preliminary experiments also showed that FPI powder was soluble in DCM and insoluble in pure HFPME. FPI is also insoluble in FDC. Thus, another polymer−solvent−nonsolvent ternary phase diagram was developed to represent the solubility of the FPI in the cosolvent, as shown in Figure 2b. As a result, we achieved a one-phase composition of FDC and FPI dissolved in the DCM-HFPME cosolvent.

Although DCM is a good solvent for FPI, neither FDC nor HFPME is suitable for FPI. Therefore, we should have avoided the nonsolvent-induced phase separation (NIPS) in the disperse phase. Therefore, we carefully determined the

(a)

FDC

HFPME

1-phase

Disperse phase composition

2-phase

DCM

(b)

DCM

FPI

solid

viscous

2-phase

1-phase

Disperse phase composition
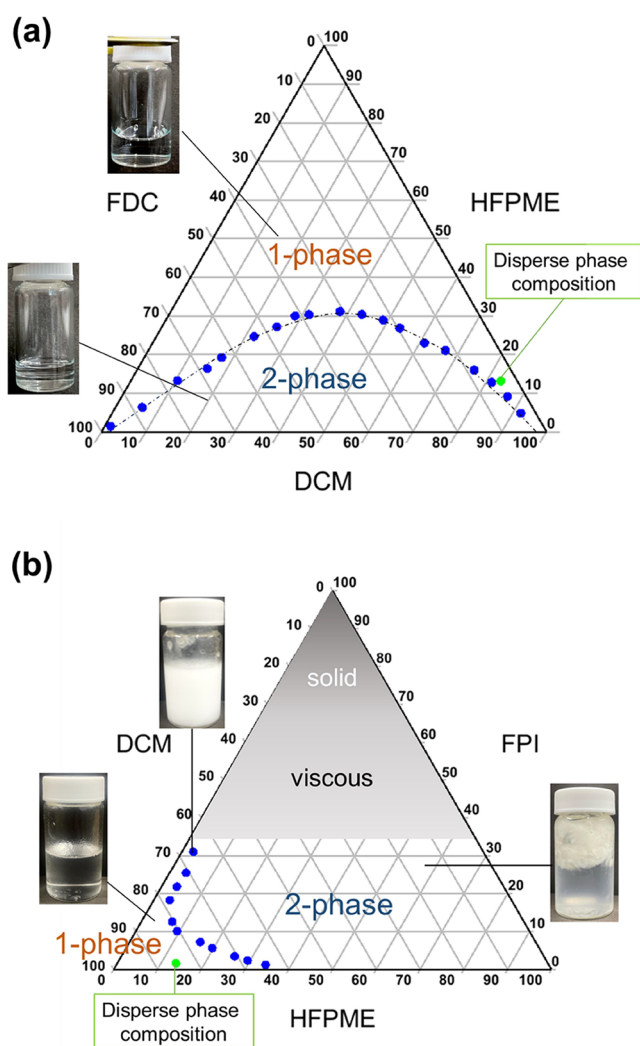
HFPME

Figure 2. Ternary phase diagrams illustrating dispersed phase compositions in (a) DCM-HFPME-FDC system and (b) DCM-HFPME-FPI system. The axes depict the weight fraction of each component in percentage. The green point on the graph signifies the operational point of our disperse phase in the SPG membrane emulsification process.

dispersed phase compositions by maximizing the DCM content according to the phase diagrams shown in Figure 2b, where all the components were perfectly dissolved and mixed into one phase.

As indicated in Figure 2a,b, the operating point of SPG membrane emulsification was selected to be in the one-phase region close to the critical boundary of phase separation. When DCM and HFPME in the emulsion evaporated after the dispersion phase was pressurized into the continuous phase, phase separation between the FDC-rich and DCM-rich phases was induced as the FDC weight fraction increased due to the evaporation of DCM and HFPME. Subsequently, solidification of the FPI occurred because of a further decrease in the solvent fraction due to continuous evaporation. As a result, depending on the immiscibility of FPI and FDC, FDC/FPI core−shell microparticles were successfully generated by EIPS and solidification processes following SPG membrane emulsification. The volume ratio of the core to the shell is an important factor in determining the core−shell structure. We designed an

optimized disperse phase with 3.6 wt % FDC and 1.5 wt % FPI.

Because low concentrations of FDC and FPI were completely dissolved in a mixture of DCM and HFPME at a 9:1 v/v ratio, the boiling point of the cosolvent was dominated by DCM, which had a lower value than that of HFPME. Thus, the solvents evaporated quickly at room temperature to generate homogeneous core−shell particles. Our production method of FPI/FDC core−shell particles based on SPG membrane emulsification was able to be scaled up within 100 times based on our current experimental setups (Figure S1), without affecting the morphology and monodispersity of the particles. On the other hand, for industrial-scaled production, the SPG membrane size was also required to be scaled up along with the dispersed and continuous-phase volume to compensate the transmembrane pressure due to the increasing hydraulic pressure in the column.

3.3. Characterization of FDC/FPI Core−Shell Microparticles. The outer and inner morphologies of the freeze-dried FDC/FPI core−shell particles were verified using SEM (Figure 3a). The cross-sectional SEM images clearly revealed the well-defined core and shell structures of these particles. Moreover, the CLSM image of the FDC/FPI suspension in water (Figure 3b) provided evidence that aligned with the findings from the SEM. An optical image of the FDC/FPI core−shell particles (Figure 3c) was obtained by dispersing them in water, revealing the morphology and dispersity of the core−shell particles in a homogeneous medium. Furthermore, because the FPI shell was fluorescently labeled with Nile red after the evaporation of DCM, the CLSM image of the suspension clearly indicated a core−shell structure. A large portion of the microparticles in Figure 3c displayed double-ring-like patterns, reflecting their concave shapes, which became evident when the core−shell particles settled on the bottom of the glass-bottom dish.

As described in the SEM, optical, and CLSM images, most FDC/FPI core−shell particles closely resembled the shape and size of human RBCs immediately after SPG membrane emulsification without additional treatments. Owing to the low amount of FPI used to encapsulate the FDC, the FPI shell acted like a deformable thin shell, protecting the FDC analogous to the RBC membrane. The size distribution of fabricated core−shell particles measured by a particle size analyzer was plotted (Figure 3e), and the average size was determined to be 7.4 μm with a coefficient of variation of 20.9%. The narrow distribution of the FDC/FPI core−shell particles is attributed to the homogeneous membrane pores of the SPG membrane.

The presence of FDC within the core of the core−shell particles was established by identifying the stretching vibration bands of FDC (1243 and 1216 cm^{-1} for −CF$_2$ and 1153 cm^{-1} for −CF$_3$) in the FT-IR spectrum of FDC/FPI core−shell particles (Figure 3d). Moreover, the characteristic peaks in the ^{19}F NMR spectrum of the FDC/FPI core−shell particles further confirmed the presence of the FDC core. These distinctive peaks of FDC were observed at chemical shifts of −117, −122, −129, −139, and −188 ppm, as illustrated in Figure 3f. Therefore, we successfully encapsulated FDC into a thin FPI shell using SPG membrane emulsification, resulting in spontaneous concave microparticles similar to those in human RBCs.

3.4. Stability and Sterilization of the Core−Shell Microparticles. To ensure the long-term storage and
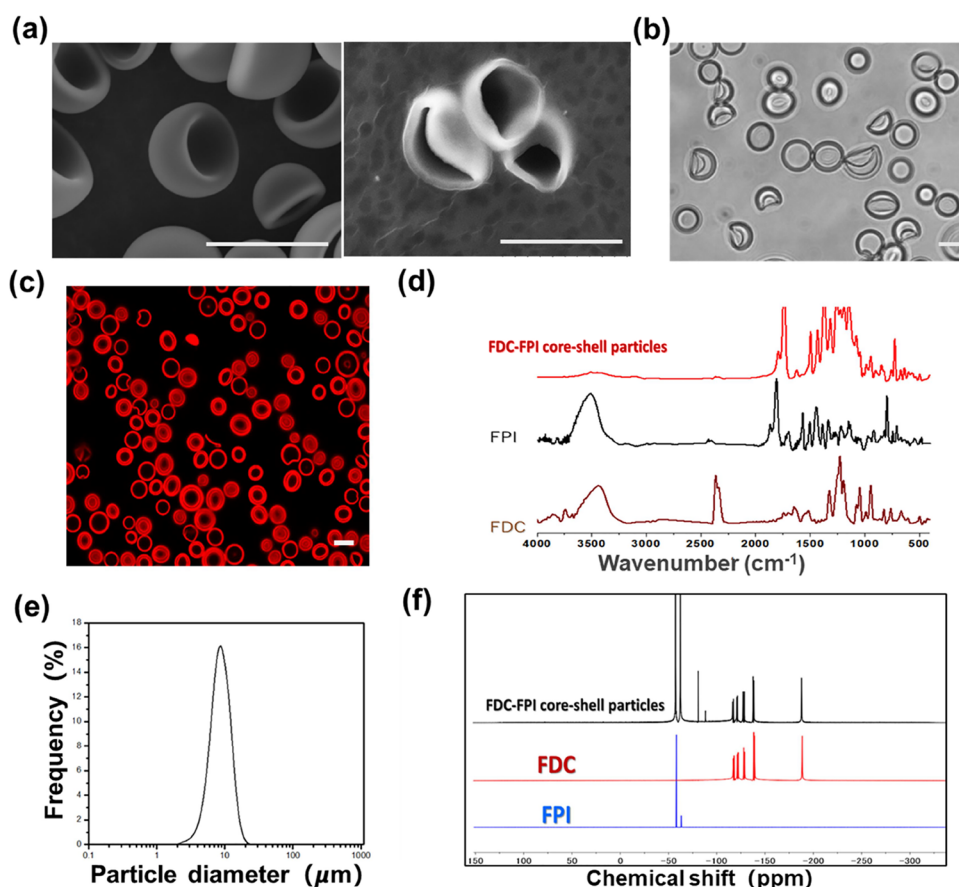
Figure 3. Characterization of FDC/FPI microparticles: (a) SEM images of FDC/FPI core−shell particles (left) and their cross sections (right); (b) optical microscopic images of FDC/FPI core−shell particle suspension; (c) CLSM images of FDC/FPI core−shell particle suspension; (d) size distribution of freeze-dried FDC/FPI core−shell particles; (e) FT-IR spectra of FDC/FPI core−shell particles, FPI, and FDC; and (f) ^{19}F NMR spectrum of FDC/FPI core−shell particles; scale bar = 10 μm.

application of particles, it is crucial for them to retain their original structure and functionality. Therefore, FPI was selected as the protective shell for FDC, focusing on its stability and oxygen permeability. To compare with a previous study by Adamczak et al. that reported the excellent thermal stability of polyimide at 530 °C,[18] we evaluated the physical and chemical stability of our FPI material, especially after fabrication. After preparing the core−shell particles, an assessment of the particle response to multiple extreme conditions was conducted to evaluate their stability and functionality.

The stability and sterilizability of the FDC/FPI core−shell particles were assessed under different harsh conditions, including pH 3−10, autoclaving, ethanol washing, and ethylene oxide sterilization. Thereafter, the structural integrity and functionality of the core−shell particles were assessed through SEM imaging, particle size distribution, and the availability of encapsulated FDC. In the size distribution assessment, no significant changes were observed in the original values. The core−shell particle morphology is also an important part of their stability and function, and no significant changes were observed before and after all treatments (Figure 4a). This inherent stability of the FPI effectively prevented the unintended release of the encapsulated core material.

The presence of the core material, FDC, was quantitatively confirmed by ^{19}F NMR spectroscopy. These findings were in full agreement with the previously mentioned stability results

and are visually depicted in Figure 4b. In addition, as demonstrated in all the SEM images in Figure 4a, no swelling, shrinking, melting, or any other physiochemical changes in the particle morphology were observed to take place. One significant advantage of FDC/FPI core−shell particles is their robustness to extreme conditions while minimizing the shell thickness to maintain deformability. Moreover, the thin shell prevented evaporation of the FDC during autoclaving. We speculate that the immiscibility of FDC and FPI contributed to the prevention of FDC loss. In other words, the FDC must obey the solution-diffusion mechanism to permeate from the core to the exterior of the shell. However, the solubility of the FDC in FPI was extremely low. Thus, once the FDC/FPI core−shell particles are formed, evaporation of FDC by permeating through the FPI shell would not occur.

The potential applications of PFC-based microparticles as oxygen carriers in tissue engineering, bioproduction using animal cells, and clinical applications require prior sterilization to avoid contamination. Autoclaving is one of the most commonly used sterilization methods. However, previously reported PLC and PDMS thermoplastic elastomer-based core−shell particles from our group were not stable under alkaline pH conditions (pH 9 or 10), and autoclaving. In comparison, the stability and sterilization of the FDC/FPI core−shell particles provided compelling evidence that FPI exhibits robust stability under various conditions. The high stability of the FDC/FPI core−shell particles suggests a wide
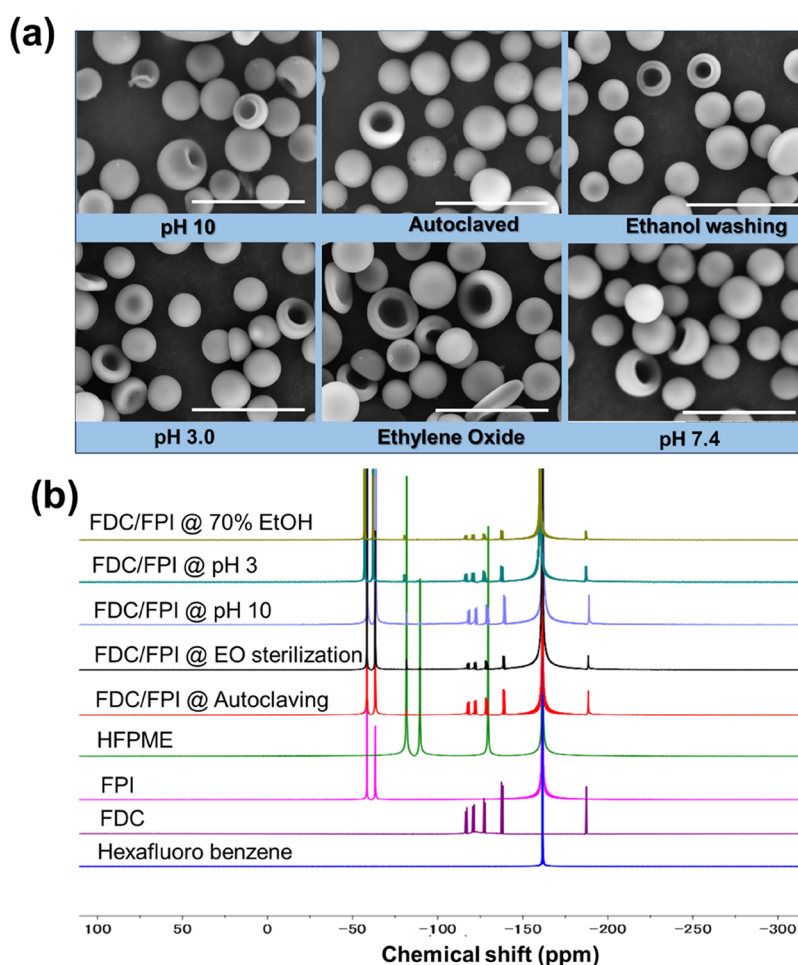
Figure 4. Stability of FDC/FPI microparticles under varied environmental conditions. (a) SEM images of FDC/FPI core–shell particles after exposure to pH 10, pH 7.4, pH 3.0, autoclaving, ethanol washing, and EO sterilization. (b) ^{19}F NMR spectrum confirming FDC presence after multiple stability and sterilization assessments. Chloroform-*d* was used to dissolve the particles, and hexafluorobenzene was added as the internal standard. Scale bar = 10 μm.

range of applications and potential for the modification of particle properties.

3.5. Oxygen Capacity of FDC/FPI Core–Shell Particles Analyzed by Oxygen Loading and Releasing Tests. Water or cell medium has poor solubility of oxygen, approximately 2 mL of O_2 per 1 mL of water at 1 atm, and room temperature.[19] In contrast, PFCs such as PFOB and FDC have much greater oxygen solubility, approximately 20–30 times that of water.[14] Under normal physiological conditions, oxygen transport occurs through the association and dissociation of hemoglobin within red blood cells, allowing them to carry and deliver oxygen.[20] Based on the solubility of oxygen in the FDC/FPI core–shell particles,[14] a suspension comprising 45 vol % FDC/FPI core–shell particles is estimated to carry 135 mL of oxygen per liter under 1 atm of pure oxygen. This oxygen-carrying capacity is comparable to that of blood, which contains approximately 201 mL of oxygen per liter.[21] Theoretically, FDC/FPI AOC microparticles should absorb and release oxygen to mimic the oxygen delivery of RBC. Thus, we dispersed our microparticles in water and perfused oxygen and nitrogen gas alternatively into the suspension to simulate the charging and discharging processes. A DO meter was used to monitor the DO values of the bulk media in real time.

Initially, both water and the AOCs were saturated with air (20% O_2) above the suspension surface and were in equilibrium with each other. After pure oxygen was bubbled at a flow rate of 100 mL min^{-1}, the bulk water was temporarily saturated with pure oxygen (100% O_2) without N_2. Because the DO meter reads the DO value of the bulk, both pure water and samples with FDC/FPI AOC microparticles would reach the same value after sufficient oxygen was bubbled through, which is the initial point of the oxygen-releasing curve. Subsequently, N_2 gas was purged at a constant rate of 100 mL min^{-1} to decrease the DO. Without the FDC/FPI AOC microparticles, the water saturated with oxygen quickly released oxygen into the air until it reached equilibrium with the vapor pressure above it, according to Henry's law. However, as shown in Figure 5, suspensions of FDC/FPI core–shell particles maintained the highest DO value for a longer period than water, and the subsequent decrease in speed was lower than that of pure water. This was because oxygen was released from the FDC/FPI core–shell particles into the bulk media for the core–shell particles to reach a new equilibrium with the reduced partial oxygen pressure applied to them. The oxygen absorption and stripping of our previously reported microsized FDC emulsion (10 vol %) are also shown in Figure S2 as a control group without a core–shell structure.
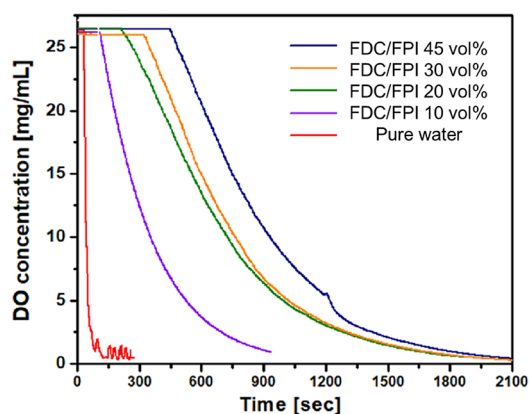
Figure 5. Dissolved oxygen release measurements from FDC/FPI core−shell particles in pure water at varying volumetric fractions (10, 20, 30, and 45%).

3.6. Oxygen Delivery of FDC/FPI Core−Shell Particles to Cells In Vitro. Based on the oxygen capacity of the FDC/FPI core−shell particles investigated in the previous sections, we assessed our hypothesis regarding the oxygen delivery function and biocompatibility of the FDC/FPI core−shell particles in cells. Thus, hr-HeLa cells were used to visualize the oxygen delivery function of the FDC/FPI core−shell particles in vitro under hypoxic conditions by expressing enhanced green fluorescent protein (EGFP) in cell culture.[9,10] We cultured the FDC/FPI core−shell particles with hr-HeLa cells under hypoxic conditions (5% O_2) for 48 h. The intensity of green fluorescence emitted by hr-HeLa cells was directly proportional to the degree of hypoxia.[17] Following the incubation period, we immediately captured a fluorescence image using CLSM to ensure that the extracellular oxygen environment remained unaffected by the atmospheric conditions. As depicted in Figure 6, the FDC/FPI core−shell particles exhibited an elevated oxygen concentration and reduced EGFP fluorescence intensity compared to the control condition. Moreover, the biocompatibility of the FDC/FPI core−shell particles was confirmed by the merged CLSM channels shown in Figure 6, where hr-HeLa cells survived close to the FDC/FPI core−shell particles without internalization of the particles.

In addition to the alternative use of packed hRBCs (PRBCs) for transfusion, AOCs show substantial potential in 3D tissue engineering applications.[22,23] Historically, extensive research has focused on nanosized AOCs,[24,25] such as Hb-encapsulated micelles/liposomes, cross-linked Hb, and polymer-conjugated Hb. FDC-based AOCs with nanometer-scale dimensions have also been investigated;[26,27] however, they suffer from short blood retention times due to rapid excretion, unlike the ∼4-month lifespan of hRBCs. Recently, a new category of AOCs has emerged based on bioinspired chemistry, with a focus on microsized AOCs for tissue engineering.[6] Our study is the first to report the fabrication of FDC-encapsulated microparticles using a synthetic polymer shell, FPI. Moreover, unlike PFOB-containing bromides, FDC is immiscible with DCM because of its high fluorosis structure. The HFPME cosolvent system developed in this study will be useful for preparing hybrid-fluorous and hydrophobic materials using a fluorous biphasic system in the field of materials chemistry.

4. CONCLUSIONS

We successfully encapsulated FDC using a highly oxygen-permeable and stable FPI, aided by a novel cosolvent system comprising DCM-HFPME and SPG membrane emulsification techniques. This was achieved without the need for additional cross-linking processes or solvent-induced shape adjustments. The FDC/FPI core−shell microparticles exhibited good oxygen-carrying capacity, morphology, stability against acid and bases, and sterilization. These properties highlight their potential utility as highly effective oxygen microcarriers for biomedical and bioproduction applications. Ultimately, our findings, along with the concept of FDC/FPI core−shell particle formulation and phase separation behavior, have promising implications for the application of PFC compounds in the field of material chemistry.

■ ASSOCIATED CONTENT

Ⓢ Supporting Information

The Supporting Information is available free of charge at https://pubs.acs.org/doi/10.1021/acsomega.4c00897.

> Figure S1: SPG membrane emulsification scale-up setup (50 times); Figure S2: Monitored oxygen release curve from a 20 vol % FDC emulsion in pure water (PDF)
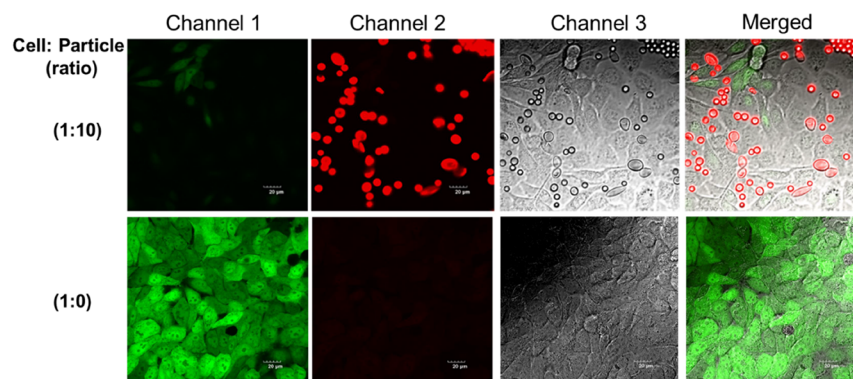
Figure 6. In vitro assessment of the oxygen delivery function of FDC/FPI core−shell particles. CLSM images of hr-HeLa cells (green) were captured from samples with and without the particles (red) under 5% O_2 after 48 h. Red channel: excitation = 561 nm, green channel: excitation = 488 nm; scale bar = 20 μm.

■ AUTHOR INFORMATION

Corresponding Author

Taichi Ito − *Department of Chemical System Engineering, The University of Tokyo, Bunkyo-ku, Tokyo 113-8656, Japan; Center for Disease Biology and Integrative Medicine, The University of Tokyo, Bunkyo-ku, Tokyo 113-0033, Japan;* orcid.org/0000-0002-1589-8242; Phone: +81-3-5841-1425; Email: itotaichi@g.ecc.u-tokyo.ac.jp

Authors

Qiming Zhang − *Department of Chemical System Engineering, The University of Tokyo, Bunkyo-ku, Tokyo 113-8656, Japan*

Natsuko F. Inagaki − *Department of Chemical System Engineering, The University of Tokyo, Bunkyo-ku, Tokyo 113-8656, Japan; Center for Disease Biology and Integrative Medicine, The University of Tokyo, Bunkyo-ku, Tokyo 113-0033, Japan;* orcid.org/0000-0002-6309-9023

Arvind K. Singh Chandel − *Department of Chemical System Engineering, The University of Tokyo, Bunkyo-ku, Tokyo 113-8656, Japan;* orcid.org/0000-0002-7130-7734

Hiromi Yoshida − *Department of Chemical System Engineering, The University of Tokyo, Bunkyo-ku, Tokyo 113-8656, Japan*

Da Xiao − *Department of Chemical System Engineering, The University of Tokyo, Bunkyo-ku, Tokyo 113-8656, Japan*

Masamichi Kamihira − *Department of Chemical Engineering, Kyushu University, Fukuoka 819-0395, Japan;* orcid.org/0000-0003-2570-5712

Tomohito Hamada − *Technology and Innovation Center, Daikin Industries Ltd., Settsu, Osaka 566-8585, Japan;* orcid.org/0000-0001-8724-8225

Shigehito Sagisaka − *Technology and Innovation Center, Daikin Industries Ltd., Settsu, Osaka 566-8585, Japan*

Yosuke Kishikawa − *Technology and Innovation Center, Daikin Industries Ltd., Settsu, Osaka 566-8585, Japan*

Complete contact information is available at:
https://pubs.acs.org/10.1021/acsomega.4c00897

Notes

The authors declare no competing financial interest.

■ REFERENCES

(1) Kim, H. W.; Greenburg, A. G. Artificial Oxygen Carriers as Red Blood Cell Substitutes: A Selected Review and Current Status. *Artif Organs* **2004**, *28* (9), 813−828.

(2) Bland, E.; Dréau, D.; Burg, K. J. L. Overcoming Hypoxia to Improve Tissue-Engineering Approaches to Regenerative Medicine. *J. Tissue Eng. Regen Med.* **2013**, *7* (7), 505−514.

(3) Xiang, Y.; Bernards, N.; Hoang, B.; Zheng, J.; Matsuura, N. Perfluorocarbon Nanodroplets Can. Reoxygenate Hypoxic Tumors *in Vivo* without Carbogen Breathing. *Nanotheranostics* **2019**, *3* (2), 135−144.

(4) Ohta, S.; Hashimoto, K.; Fu, X.; Kamihira, M.; Sakai, Y.; Ito, T. Development of Human-Derived Hemoglobin−Albumin Microspheres as Oxygen Carriers Using Shirasu Porous Glass Membrane Emulsification. *J. Biosci Bioeng* **2018**, *126* (4), 533−539.

(5) Sen gupta, A. Hemoglobin-Based Oxygen Carriers: Current State-of-the-Art and Novel Molecules. *Shock* **2019**, *52*, 70−83. Lippincott Williams and Wilkins October 1.

(6) Zhang, Q.; Inagaki, N. F.; Ito, T. Recent Advances in Micro-Sized Oxygen Carriers Inspired by Red Blood Cells. *Sci. Technol. Adv. Mater.* **2023**, *24* (1), No. 2223050, DOI: 10.1080/14686996.2023.2223050.

(7) Jia, Y.; Duan, L.; Li, J. Hemoglobin-Based Nanoarchitectonic Assemblies as Oxygen Carriers. *Adv. Mater.* **2016**, *28* (6), 1312−1318.

(8) Okamoto, W.; Hasegawa, M.; Kohyama, N.; Kobayashi, T.; Usui, T.; Onozawa, H.; Hashimoto, R.; Iwazaki, M.; Kohno, M.; Georgieva, R.; Bäumler, H.; Komatsu, T. Core−Shell Structured Hemoglobin Nanoparticles as Artificial O_2 Carriers. *ACS Appl. Bio Mater.* **2022**, *5* (12), 5844−5853.

(9) Fu, X.; Ohta, S.; Kawakatsu, T.; Kamihira, M.; Sakai, Y.; Ito, T. Bioinspired Perfluorocarbon-Based Oxygen Carriers with Concave Shape and Deformable Shell. *Adv. Mater. Technol.* **2022**, *7* (3), No. 2100573, DOI: 10.1002/admt.202100573.

(10) Zhang, Q.; Inagaki, N. F.; Yoshida, H.; Kamihira, M.; Sakai, Y.; Ito, T. Development of Erythrocyte-Mimetic PFOB/PDMS Thermoplastic Elastomer Core-Shell Microparticles via SPG Membrane Emulsification. *J. Membr. Sci.* **2024**, *689*, No. 122119.

(11) Kapantaidakis, G. C.; Koops, G. H. High Flux Polyethersulfone−Polyimide Blend Hollow Fiber Membranes for Gas Separation. *J. Membr. Sci.* **2002**, *204* (1−2), 153−171.

(12) Mikawa, M.; Nagaoka, S.; Kawakami, H. Gas Transport Properties and Molecular Motions of 6FDA Copolyimides. *J. Membr. Sci.* **1999**, *163* (2), 167−176.

(13) Yoshioka, T.; Kojima, K.; Shindo, R.; Nagai, K. Gas-separation Properties of Amine-crosslinked Polyimide Membranes Modified by Amine Vapor. *J. Appl. Polym. Sci.* **2017**, *134* (10), 44569.

(14) Jägers, J.; Wrobeln, A.; Ferenz, K. B. Perfluorocarbon-Based Oxygen Carriers: From Physics to Physiology. *Pflugers Arch* **2021**, *473* (2), 139−150.

(15) Mohanto, N.; Park, Y.-J.; Jee, J.-P. Current Perspectives of Artificial Oxygen Carriers as Red Blood Cell Substitutes: A Review of Old to Cutting-Edge Technologies Using in Vitro and in Vivo Assessments. *J. Pharm. Investig* **2023**, *53*, 153.

(16) Fu, X.; Ohta, S.; Kamihira, M.; Sakai, Y.; Ito, T. Size-Controlled Preparation of Microsized Perfluorocarbon Emulsions as Oxygen Carriers via the Shirasu Porous Glass Membrane Emulsification Technique. *Langmuir* **2019**, *35* (11), 4094−4100.

(17) Ono, A.; Ito, A.; Sato, T.; Yamaguchi, M.; Suzuki, T.; Kawabe, Y.; Kamihira, M. Hypoxia-Responsive Transgene Expression System Using RTP801 Promoter and Synthetic Transactivator Fused with Oxygen-Dependent Degradation Domain. *J. Biosci Bioeng* **2017**, *124* (1), 115−124.

(18) Adamczak, A. D.; Spriggs, A. A.; Fitch, D. M.; Awad, W.; Wilkie, C. A.; Grunlan, J. C. Thermal Degradation of High-temperature Fluorinated Polyimide and Its Carbon Fiber Composite. *J. Appl. Polym. Sci.* **2010**, *115* (4), 2254−2261.

(19) Newby, D.; Marks, L.; Lyall, F. Dissolved Oxygen Concentration in Culture Medium: Assumptions and Pitfalls. *Placenta* **2005**, *26* (4), 353−357.

(20) Nicolaides, A. N.; Horbourne, T.; Bowers, R.; Kidner, P. H.; Besterman, E. M. BLOOD VISCOSITY, RED-CELL FLEXIBILITY, HÆMATOCRIT, AND PLASMA-FIBRINOGEN IN PATIENTS WITH ANGINA. *Lancet* **1977**, *310* (8045), 943−945.

(21) Stein, T. R.; Martin, J. C.; Keller, K. H. Steady-State Oxygen Transport through Red Blood Cell Suspensions. *J. Appl. Physiol.* **1971**, *31* (3), 397−402.

(22) Lee, H.-Y.; Kim, H.-W.; Lee, J. H.; Oh, S. H. Controlling Oxygen Release from Hollow Microparticles for Prolonged Cell Survival under Hypoxic Environment. *Biomaterials* **2015**, *53*, 583−591.

(23) Radisic, M.; Deen, W.; Langer, R.; Vunjak-novakovic, G. Mathematical Model of Oxygen Distribution in Engineered Cardiac Tissue with Parallel Channel Array Perfused with Culture Medium

Containing Oxygen Carriers. *American Journal of Physiology-Heart and Circulatory Physiology* **2005**, *288* (3), H1278−H1289.

(24) Alayash, A. I. Oxygen Therapeutics: Can We Tame Haemoglobin? *Nat. Rev. Drug Discov* **2004**, *3* (2), 152−159.

(25) Gao, M.; Liang, C.; Song, X.; Chen, Q.; Jin, Q.; Wang, C.; Liu, Z. Erythrocyte-Membrane-Enveloped Perfluorocarbon as Nanoscale Artificial Red Blood Cells to Relieve Tumor Hypoxia and Enhance Cancer Radiotherapy. *Adv. Mater.* **2017**, *29* (35), No. 1701429, DOI: 10.1002/adma.201701429.

(26) Cheng, Y.; Cheng, H.; Jiang, C.; Qiu, X.; Wang, K.; Huan, W.; Yuan, A.; Wu, J.; Hu, Y. Perfluorocarbon Nanoparticles Enhance Reactive Oxygen Levels and Tumour Growth Inhibition in Photodynamic Therapy. *Nat. Commun.* **2015**, *6* (1), 8785.

(27) Hu, H.; Yan, X.; Wang, H.; Tanaka, J.; Wang, M.; You, W.; Li, Z. Perfluorocarbon-Based O_2 Nanocarrier for Efficient Photodynamic Therapy. *J. Mater. Chem. B* **2019**, *7* (7), 1116−1123.